NSRRC-J04799 (2015)

CHEMISTRY OF MATERIALS

Article

pubs.acs.org/cm

Shape and Confinement Effects of Various Terminal Siloxane Groups on Supramolecular Interactions of Hydrogen-Bonded Bent-Core Liquid Crystals

I-Hung Chiang,[†] Wei-Tsung Chuang,*[,‡] Chia-Lin Lu,[†] Ming-Tao Lee,[‡] and Hong-Cheu Lin*[,†]

[†]Department of Materials Science and Engineering, National Chiao Tung University, Hsinchu 30049, Taiwan

[‡]National Synchrotron Radiation Research Center, Hsinchu, 30076, Taiwan

Supporting Information

ABSTRACT: To investigate the shape and confinement effects of the terminal siloxane groups on the self-assembled behavior of molecular arrangements in hydrogen-bonded (H-bonded) bent-core complexes, four H-bonded bent-core complexes **S1**, **P1**, **C4**, and **P8** with string-, ring-, and cage-like siloxane termini (i.e., linear siloxane unit −Si−O−Si−O−Si−, cyclic siloxane unit $(Si-O)_4$, and silsesquioxane unit POSS, respectively) were synthesized and investigated. By X-ray diffraction measurements, different types of SmCG (B8) phases and leaning angles were controlled by the shape effect of the string- and cage-like siloxane termini for **S1** and **P1** (with only one arm of H-bonded bent-core), respectively. In addition, the confinement effect of **P1**, **C4**, and **P8** (accompanied by increasing the numbers of attached H-bonded bent-core arms) resulted in higher transition temperatures and the diminishing of mesophasic ranges (even the disappearance of mesophase in **P8**). Moreover, AFM images showed the bilayer smectic CG phases of **S1** and **P1** were aligned to reveal highly ordered thread-like structures by a DC field. By spontaneous polarization measurements within the mesophasic ranges, **S1** and **P1** showed ferroelectric transitions but **C4** displayed antiferroelectricity. Finally, the electro-optical performance of B8 phases could be optimized through binary mixtures of **S1** and **P1**, and a well aligned modulated ribbon phase could be formed via specific molar ratios of the binary mixtures.

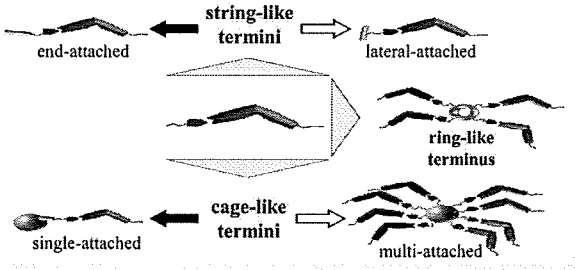

INTRODUCTION

Bent-core or banana-shaped liquid crystals (LC) were first synthesized and investigated by Vorländer et al. in 1932.[1,2] Since the discovery of their special electro-optical properties by Niori et al.,[3] many scientists became interested in the complicated mesophasic behavior, molecular biaxiality, layer polarity, and supramolecular chirality of achiral bent-core molecules.[4−7] These excellent electro-optical properties and structural characteristics might enable many applications, e.g., fast responsive LC displays,[8,9] light-scattering LC displays,[10] storage devices,[11] nonlinear optical appliances,[12] biosensors,[13] piezoelectric objects,[14] charge-generation interfaces,[15] blue-phase materials,[16,17] supramolecular complexes,[18−20] biaxial mesogens,[21,22] and tunable chromophores.[23]

On the basis of texture features and the results of X-ray diffractions, eight mesophases with smectic or columnar or three-dimensional orders, namely B1, B2, ..., B8 in chronological order, have been found in bent-core LCs with the effects of their configurations, including the zenithal constituents, the shapes of the rigid cores, the lengths of the flexible chains, and the roles of substituents at selected positions of rigid cores, on the properties of LCs.[6,7,24−27] As a result of the splay of polarization in smectic layers,[28] the modulation induces the breaking layers or ribbons to undergo long-range ordering in two-dimensional (2D) lattices of oblique (Col_{ob}), rectangular (Col_r), or hexagonal (Col_h) packing, classified as the B1 phase.[29] Depending upon the direction of polarization in the continuous layers and the molecular tilt angle with respect to the layer normal, the bent-core molecules spontaneously exhibit polar and chiral layers, leading to SmCP phases (B2) having four layer-type structures with a ferroelectric or antiferroelectric state, homochiral phases of SmC_SP_F and SmC_aP_A along with racemic phases SmC_aP_F and SmC_SP_A.[3,30] The B3 phase generally features a highly ordered smectic structure;[31−33] the B4 phase typically represents a soft crystalline mesophase with a TGB-like helical organization of smectic layers.[34,35] Smectic monolayers with in-plane order are designated as the B5 phase,[24,36] whereas intercalated smectic structures without in-plane orders have the characteristics of the B6 phase.[37,38] The B7 phase, as an undulated smectic phase, ordinarily exhibits a characteristic morphology of helical filaments.[39−42]

A doubly tilted smectic phase possessing a chiral C1 symmetry configuration, assigned to a SmCG phase first proposed by de Gennes et al.,[43] is named the B8 phase.[6,7,44−50]

Received: January 5, 2015
Revised: May 31, 2015
Published: June 1, 2015

 © 2015 American Chemical Society

DOI: 10.1021/acs.chemmater.5b00033
Chem. Mater. 2015, 27, 4525−4537

As illustrated in Figure 1, two set angles (ω and Ψ) are defined with respect to the layer normal: the tilt of the molecular plane

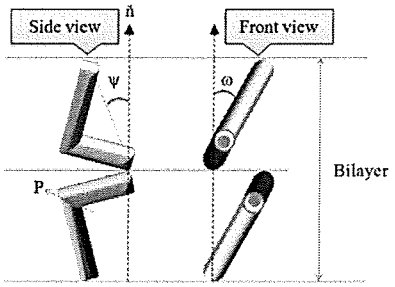

Figure 1. Schematic representation of the B8 phase. Ψ: leaning angle; ω: tilt angle; P: polar direction; $\check{n}$: layer normal.

(clinicity: ω) and the tilt of the molecular kink direction (leaning: Ψ). The B8 phase is suggested to relate to the deflection of the center of the molecular mass in bilayers with an asymmetric molecular configuration.[51] On the basis of these conformational varieties, Brand et al.[47] proposed that eight orientations of bent-core molecules are possible for molecular packing in the B8 phase, but few experiments are reported regarding the realization of the B8 phase in bent-core molecules. We found the rare B8 phase in a new H-bonded bent-core complex bearing a lateral-attached siloxane terminal unit and determined the leaning and tilt angles of the SmCG-type phases using synchrotron-based in situ small-angle X-ray scattering (SAXS) and wide-angle X-ray scattering (WAXS) measurements under DC electric fields.[51] With several SmCG (B8)-type phase transitions from modulated bilayers to monolayers ($Sm\tilde{C}_{ob}G_2P_F$—$USmCG_2P_A$—$SmCG_2P_F$—$SmCGP_F$), we speculated that the interactions between the competition of hydrogen bonds and nanosegregation of the siloxane units play important roles in bent-core complexes in the B8 phase, but it remained unclear what other kinds of driving forces could induce the B8 phase and how to manipulate the B8 phase via the molecular designs of bent-core complexes.

Inspired by previous research,[51,52] we expanded various types of terminal siloxane groups in these hydrogen-bonded (H-bonded) bent-core complexes to investigate the shape effects of the terminal siloxane groups on the self-assembled behavior of molecular arrangements, including the bilayer structures of the B8 phase. As demonstrated in Figure 2, the H-bonded bent-core complexes are attached to various terminal siloxane groups with string-, ring-, and cage-like shapes. We believe that understanding the influence of various terminal siloxane groups with different shapes and confinements would allow us to resolve the significant competing interactions between hydrogen bonding and siloxane segregation in the structural formation of H-bonded bent-core complexes. Herein, the delicate balance between these two forces might lead to different self-assembled structures of the H-bonded bent-core molecules, where the electro-optical properties of these mesophases, including the B2 (SmCP) or B8 (SmCG) phases, can be further explored in this study.

EXPERIMENTAL SECTION

Synthesis. The components for the synthesis of bent-core complexes **S1-COOH**, **P1-COOH**, **C4-COOH**, **P8-COOH**, and **NBF14** are listed in Scheme S1 of the Supporting Information. The details of synthetic steps and the elemental characterization of **S1-COOH**, **P1-COOH**, **C4-COOH**, **P8-COOH**, and **NBF14** are also shown in the Supporting Information.

Characterization. ^1H and ^{13}C NMR spectra (Varian Unity 300 MHz spectrometer; solvents D_6-DMSO, D-THF, and $CDCl_3$) and mass spectra (Micromass TRIO-2000 GC-MS) are shown in the Supporting Information. Elemental analyses (PerkinElmer 240C elemental analyzer), mesophasic patterns (polarizing optical microscope or POM, Leica DMLP; equipped with a hot stage, Linkam TMS-94/LTS350), mesophase transition temperatures, enthalpies of mesophase transitions (differential scanning calorimeter or DSC, PerkinElmer Diamond; rate 10 °C/min of heating or cooling), and

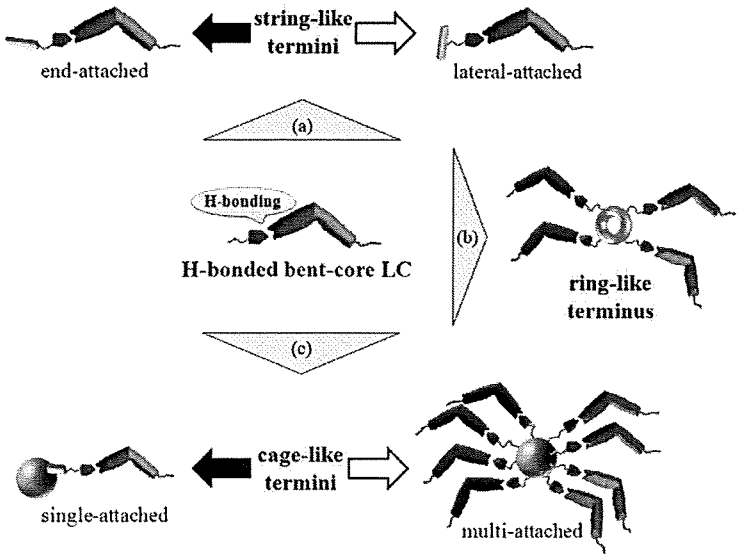

Figure 2. Schematic representation of the H-bonded bent-core complexes with the attachment of various siloxane terminal groups, i.e., (a) string-like (solid arrow: end-attached terminus; open arrow: lateral-attached)[51] termini, (b) ring-like terminus, and (c) cage-like (solid arrow: single-attached; open arrow: multiattached) termini.

DOI: 10.1021/acs.chemmater.5b00033
Chem. Mater. 2015, 27, 4525−4537

infrared spectra (at beamline BL14A1, National Synchrotron Radiation Research Center, NSRRC, Taiwan) were measured with the indicated instruments. Topology was investigated by an atomic-force microscope (AFM, Veeco diInnova, scanning rate 3 to 4 Hz). The sample was prepared in an in-plane-switching cell with 0.8 DCV/μm at 117 °C and then quenched rapidly in liquid nitrogen (less than 1 s). Small- and wide-angle X-ray scattering (SAXS/WAXS), including grazing-incidence X-ray scattering (GIWAXS/GISAXS) with synchrotron radiation were measured at beamlines BL23A, BL01C2, and BL13A1 endstations of NSRRC, respectively. Typical scattering patterns were collected from 10 to 300 s to record sufficient scattering signals with marCCD165 or mar345 image plates as detectors for SAXS and WAXS, respectively. The beam diameter was 0.5 mm for the 10-keV beam (λ = 0.124 nm^{-1}). The scattering angles were calibrated with two standard samples of silver behenate and silicon. The synthesized compounds were dropped on vertically aligned glass substrates for the GISAXS and GIWAXS measurements. With an X-ray scattering measurement in situ consisting of alignment in an electric field, the samples were sandwiched between two stainless-steel electrodes of thickness 1 mm, separated with a controlled gap 0.5 to 1 mm, and heated on a hot stage made of copper and ceramic. Within the electrodes, compounds were heated above a temperature onset of the isotropic phase and held for at least 2 min to ensure the isotropic state. After cooling to a designed temperature, a DC electric field 0.8 V/μm was applied across two electrodes, where the incident X-rays were normal to the direction of the DC field.

Electron density maps were carried out using the general Fourier formula for 2D electron density as $\rho(x,y) = \sum_{hk}(I(hk))^{1/2} \exp[2\pi i(hx + ky) + i\varphi(kh)]$, where $\varphi(hk)$ values are phases of structure factor (equal to 0 or π) and $I(hk)$ values are intensities of Bragg peaks obtained from the SAXS patterns after background subtraction and correlation of Lorentz and polarization factors. The relative values for reconstruction of electron density maps are listed in Tables S1–S3 of the Supporting Information.

Rheological measurements were proceeded by a rheometer (Anton Paar MCR 501) with a cone–plate setup. On cooling from the isotropic state at 3 °C/min, a sample was sheared at rate 1 s^{-1}, and the storage modulus (G') was recorded. Dielectric spectra were recorded over a frequency range of 0.5–1 M Hz with an impedance analyzer (Solartron 1260). The electro-optical properties were measured in commercially nonrubbed indium–tin-oxide (ITO) cells (mesophase state; thickness 9 μm; active area 0.25 cm^2) with a digital oscilloscope (Tektronix TDS-3012B) connected to a high-power amplifier (Gwinstek) and a function generator (Tektronix AFG 3021) (see the Supporting Information, Figure S1). Measurements[53] of spontaneous polarization were made with a triangular-wave method at a frequency of 300 Hz.

RESULTS AND DISCUSSION

Molecular Structure and Phase Behavior of Synthesized Complexes. As shown in Figure 3, our H-bonded bent-core complexes were designed and synthesized to possess the molecular structures of single bent cores (denoted as **S1** and **P1**) and multiple bent cores (denoted as **C4** and **P8**). An H-bonded bent-core LC complex **S1** was obtained from a proton donor **S1-COOH** containing an end-attached linear siloxane unit (–Si–O–Si–O–Si–) and a bent-core proton acceptor **NBF14** in a 1:1 molar ratio. Another multiple bent-core LC complex **C4** was obtained from a proton donor **C4-COOH** containing a ring-like siloxane unit with four –COOH groups and a bent-core proton acceptor **NBF14** in a 1:4 molar ratio. In addition, an H-bonded bent-core LC complex **P1** was obtained from a proton donor **P1-COOH** with a cage-like terminal silsesquioxane unit (POSS) and a bent-core proton acceptor **NBF14** in a 1:1 molar ratio. Another multiple bent-core complex **P8** was obtained from a multiple proton donor **POSS8-COOH** containing a cage-like POSS with eight

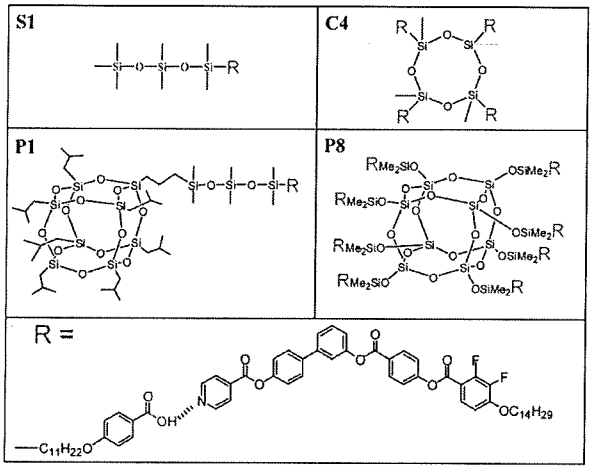

Figure 3. Molecular structures of H-bonded bent-core complexes with string-like terminus **S1**, ring-like terminus **C4**, and cage-like termini **P1** and **P8**.

–COOH groups and a proton acceptor **NBF14** in a 1:8 molar ratio. These designed H-bonded bent-core complexes were analyzed via DSC, rheology, POM, and GISAXS experiments to probe their physical properties. The temperatures and enthalpies of the phase transitions of these four compounds, obtained from DSC or POM or GISAXS, are listed in Table 1, and the crystallographic unit cell parameters are listed in Table S1 of the Supporting Information.

Table 1. Phase Transition Temperatures and Enthalpies of S1, P1, C4, and P8 upon Cooling

compd	phase transition temperature/°C [enthalpy/J/g][a]
S1	Iso 130.9[–29.8], $Sm\tilde{C}_{ob}G_2P_F$ 118.0,[b] $Sm\tilde{C}_rG_2P_F$ 105.5,[b] $SmCG_2P_F$ 80.0[–17.2], Cr
H-SiO[c]	Iso 132.1[–28.6], $Sm\tilde{C}G_2P_F$ 115.0, $USmCG_2P_A$ 97.0, $SmCG_2P_F$ 86.0, $SmCGP_F$ 75.9[–22.8], Cr
C4	Iso 150.1[–32.5], $SmCP_A$ 123.2[–14.8], Cr
P1	Iso 128.5[–5.2], $Sm\tilde{C}_{ob}G_2P_F$ 93.5[–5.9], Cr
P8	Iso 144.9[–30.6], Cr

[a]The phase transitions were measured by DSC at the first cooling scan with a rate of 10 °C/min at onset. [b]Mesophases and transition temperatures were obtained from GISAXS coupled with spontaneous polarization measurements. Cr = crystal solid; $Sm\tilde{C}_{ob}G_2P_F$ = modulated ferroelectric bilayer smectic CG phase (oblique columnar); $Sm\tilde{C}_rG_2P_F$ = modulated ferroelectric bilayer smectic CG phase (pseudorectangular oblique columnar); $SmCG_2P_F$ = ferroelectric bilayer smectic CG phase; $SmCP_A$ = antiferroelectric smectic C phase; Iso = isotropic phase. [c]Mesophases and transition temperatures are obtained from our previous report.[51]

Both H-bonded bent-core LC complexes **H-SiO**[51] and **S1** possess a similar phase sequence of spontaneous polar ordered SmCG-type owing to the comparable interactions between the hydrogen bonding and the nanosegregations of lateral- and end-attached string-like siloxane groups in **H-SiO** and **S1**, respectively. With the ring-like siloxane group to confine four H-bonded bent-cores in **C4**, the effective interactions between the nanosegregation of cyclic siloxane groups are stronger than the former (lateral- and end-attached) string-like siloxane groups in **H-SiO** and **S1**. Hence, due to both ring-like shape of the siloxane group and confinement effect of the four-armed H-

DOI: 10.1021/acs.chemmater.5b00033
Chem. Mater. 2015, 27, 4525–4537

bonded bent-cores, **C4** displayed a higher isotropization (and crystallization) temperature and a larger interaction of ring-shaped siloxane group in $SmCP_A$ phase than **H-SiO** and **S1**. The single $Sm\tilde{C}_{ob}G_2P_F$ phase in **P1** with a single-attached H-bonded bent-core was stabilized by the stronger nano-segregation of a large cubic POSS unit with the cage-like shape in contrast to **S1**, which induced the higher crystallization temperature of **P1**. Moreover, **P1** has a broader mesophasic range than **C4** due to a larger confinement effect of **C4** with four-armed H-bonded bent-cores. Based on DSC and X-ray data (shown in Figure S2 of the Supporting Information), **P1** with a single-attached H-bonded bent-core has a smaller molecular weight and a lower crystallinity to induce lower transition (melting and isotropization) temperatures than **C4**. However, **P8** possessing multiattached H-bonded bent-cores is restricted by the strongest confinement effect to bear tough steric hindrance and thus to induce the disappearance of mesophase. Also the results of second heating and first cooling of all compounds based on GISAXS, DSC, and spontaneous polarization measurements are prepared, and all complexes (except **P8**) display ferroelectric or antiferroelectric properties with enantiotropic phase transitions (see Table S4 in the Supporting Information).

Effects of Terminal Siloxane Groups on SmCG Phases. With the same characterization technique reported previously for probing the SmCG phase,[51] **S1** showed a series of subphases of SmCG types upon cooling—a modulated ferroelectric bilayer smectic CG phase with an oblique lattice ($Sm\tilde{C}_{ob}G_2P_F$), a modulated ferroelectric bilayer smectic CG phase with a pseudorectangular oblique lattice ($Sm\tilde{C}_rG_2P_F$), and a ferroelectric bilayer smectic CG phase ($SmCG_2P_F$); the superscript symbol ~ denotes modulation, and the subscript symbol 2 denotes bilayer (see Figures S3 and S4 and experimental electron density maps of **S1** in the Supporting Information). Similar to **H-SiO**, the leaning angle of **S1** decreased from approximately 56° to 51° on temperature decreasing from 125 to 85 °C, whereas the tilt angle remained constant, ca. 33° (see Figure S4, which are also listed in Table 2). Similar to **H-SiO**[51] (with a lateral-attached string-like siloxane terminus), **S1** possessing an end-attached string-like siloxane terminus was found to have a series of sub-SmCG type phases upon cooling. However, with the slight different configuration of the siloxane unit, **S1** showed the modulated ferroelectric bilayer smectic CG phase with a pseudorectangular oblique lattice ($Sm\tilde{C}_rG_2P_F$). The lattice parameters of **S1** are close to those of **H-SiO** in the same phases (i.e., $Sm\tilde{C}_{ob}G_2P_F$, see the illustration of Figure S3 in the Supporting Information). Hence, both **S1** and **H-SiO** (with end- and lateral-attached string-like siloxane termini, respectively) have analogous results of molecular structures, phase behaviors, and lattice parameters. Notably, in the hydrogen-bonding complexes **S1** and **H-SiO** the unusual phenomenon—no transition enthalpy for the series of SmCG phase transitions (see Figure S3c)—is attributed to the change of leaning angles, whereas the columnar-to-smectic transitions appeared a small transition enthalpy in covalently connected cases of silylated bent-core molecules.[54,55] Although the DSC trace can not reflect the subphase transitions of SmCG, other dynamic measurements, such as rheology and dielectric spectra, can detect these subphase transitions (see Figure S3d and the proceeding "Dielectric Relaxation of Mesophases" section).

Unlike the series of SmCG phase transitions in **S1**, complex **P1** bearing one terminal group of a large cubic POSS unit with the cage-like shape exhibited a single LC phase over the entire mesophasic temperature range as demonstrated in the GISAXS pattern and dynamic shear modulus G' in Figure 4. The

Table 2. Tilt and Leaning Angles of S1 and P1 as a Function of Temperature

temp/°C	tilt angle/deg	leaning angle/deg
S1		
125	33	56
110	33	53
100	33	52
95	33	51
P1		
125	30	55
120	30	66
110	30	68

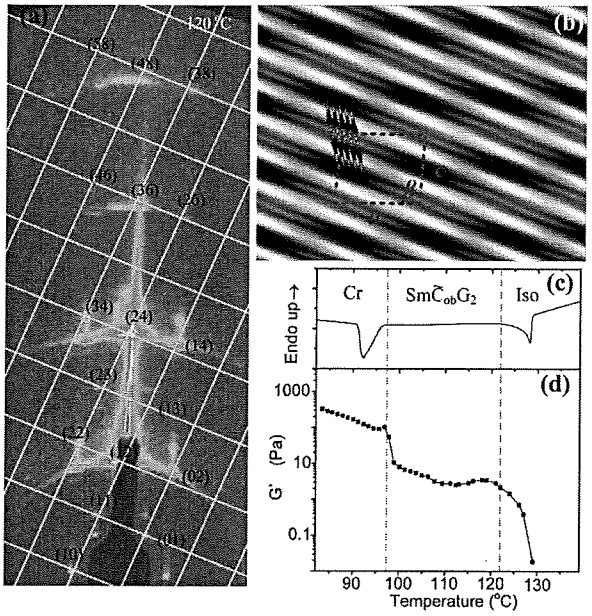

Figure 4. (a) 2D GISAXS pattern of **P1** at 120 °C; (b) electron density maps obtained by the reversed Fourier transform of GISAXS (a). The brightness reflects the higher electron density. Cartoon for molecular model: yellow, pink, blue, and green indicate siloxane units, alkyl spacers, alkyl chains, and aromatic cores, respectively. (c), (d) DSC trace and G' versus temperature upon cooling.

dynamic shear modulus G' (Figure 4d) curve shows the transition temperatures of Iso-LC and LC-Cr at 129 and 96 °C, respectively, which are consistent with the two exothermic onsets in the DSC trace in Figure 4c. We indexed all reflections in the GISAXS pattern of **P1** as an oblique lattice with two lattice parameters (a = 19.86 nm and c = 16.29 nm) and an oblique angle (β = 97°), in Figure 4a. According to the doubly tilted conformation, the tilt and leaning angles for complex **P1**, extracted from azimuthal scans of the diffuse halo at q = 12.73 nm^{-1} in the GIWAXS and E-WAXS patterns (in the Supporting Information, Figure S6), are listed in Table 2. Upon decreasing temperature, the tilt angle maintained nearly constant, about 30°, but the leaning angle increased from 55° to 68°. The same d-spacing value with and without electric field

DOI: 10.1021/acs.chemmater.5b00033
Chem. Mater. 2015, 27, 4525−4537

for **P1** (obtained from SAXS of Figure S9 in the Supporting Information) manifests that the LC domains were merely oriented along the electric-field direction, with no changes of local LC structures, such as tilt and leaning angles. Considering the bilayer thickness slashed by the large tilt and leaning angles, we reasonably infer that defect zones presumably exist in the modulated bilayers packing, as illustrated in black domains in the electron density map (Figure 4b), due to the packing frustration or splay polarization of these bent-core molecules.[7,56]

As shown in Figures 4b and S3a′, the electron density maps, which were constructed from the SAXS data by the inverse Fourier transform, obviously exhibit the modulated ribbon phases with bilayer packing in the SmCG phases of **S1** and **P1**. Thus, the bilayer packings of bent-core compounds could result in four separated sublayers, which were composed exclusively of siloxane units, alkyl end-chains, alkyl spacers, and aromatic cores (as schematically illustrated in Figure 4b). In 1D WAXS profiles of **S1** and **P1** (Figures S4c and S6c) an additional inner diffuse scattering maximum at ca. q = 5–9 nm^{-1} can be assigned to a mean distance between siloxane units in the distinct sublayers.[7] Notably, in the case of **P1** (Figure S6d) the intense inner diffuse scattering hump concentrated on the meridian at q = 5.77 nm^{-1} (d = 10.9 Å) reveals segregation of the POSS units with partial intercalation in the distinct sublayers, which might effectively alleviate an inherent steric effect of **P1** for the bilayer packing (Figure S8). Our finding is also in agreement with the bilayer packing model in covalent bent-core molecules with rigid cyclic siloxane ends reported by Tschierske's group.[52] The formation of bilayer structures in the SmCG-type phases of H-bonded bent-core complexes is easily understandable, as the hydrogen bonding enhances the tendency of segregation and the double-tilted molecular orientation with increasing a cross sectional area, which allows the molecules to wedge tightly to compensate the difference of volume within the sublayers. With the assuming complete miscibility between alkyl chains and silyl units, the antiparallel packing can directly eliminate the steric effect of silyl units, leading to monolayers as usually observed for covalently connected monosilylated bent-core compounds.[7,67,78]

The temperature dependence of the leaning angles in **P1** exhibited a tendency opposite to that of **S1**. This condition seems to imply that the size of siloxane terminal groups in the bent-core complexes has an important effect on the molecular conformation of the SmCG-type phases. The change of leaning angle can be attributed to the competition between hydrogen bonds and the nanosegregation of the siloxane group.[51] We must, at this point, clarify the relation between the stability of the hydrogen bonds and the nanosegregation of the siloxane terminal groups. Figures 5a and 5b show infrared spectra recorded upon cooling from the isotropic phase for **S1** and **P1**. Upon decreasing temperature, the shifts of two bands associated with the O–H and C=O bonds confirm the formation of hydrogen bonds between the carboxylic acid groups and the pyridyl groups for **S1** and **P1**. When the system approached the isotropic phase, weakening of the hydrogen bonds occurred: the C=O band shifted to larger wavenumber, and the signals of the O–H bond became weaker and broader.[57]

In the case of **S1** (Figure 5a), the characteristic band about 1050 cm^{-1} for the Si–O bond shifted toward a smaller wavenumber at a higher temperature, presumably because of the enhanced nanosegregation of linear siloxane units upon

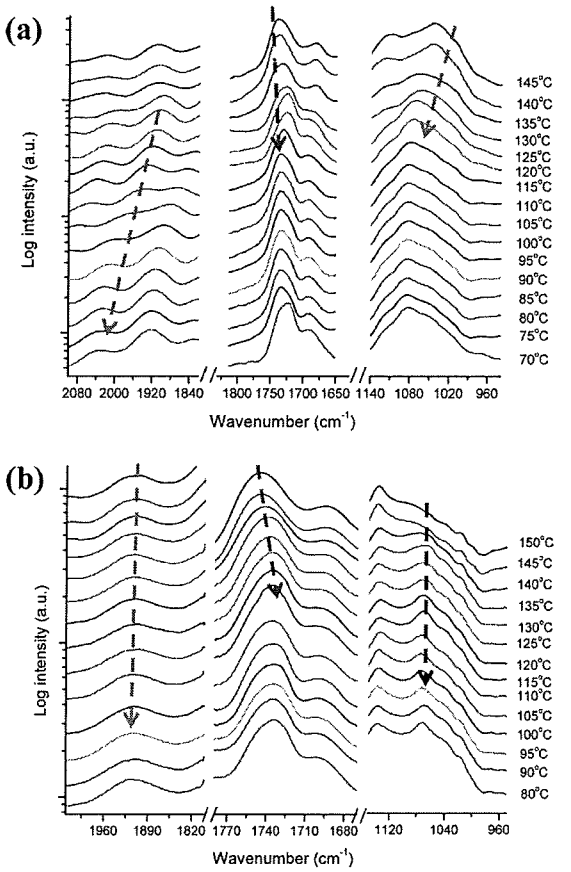

Figure 5. Infrared spectra of complexes (a) **S1** and (b) **P1**. Arrows indicate the bands shifted to higher (blue), lower (red), and the same (black) wavenumbers.

weakening of hydrogen bonds.[58] We hence suggest that the tunable interactions between the hydrogen bonding and the nanosegregation of linear siloxane groups induced the variation of the leaning angles in the SmCG-type phase transitions. As shown in Figure 6a, **S1** possessing reinforced hydrogen bonding and nanosegregation of siloxane groups upon cooling produced a decreasing distance between molecules (i.e., **S1-COOH** and **NBF14**) and resulted in a declined leaning angle upon cooling.

In contrast, the infrared spectra of the constant peak for Si–O bond in **P1** (Figure 5b) reveal the invariant strength of nanosegregation of the rigid POSS at the measured temperatures, so the strong nanosegregation of POSS terminus in **P1** dominated the molecular conformation of the SmCG phase. Considering the flexibility of the string-like siloxane group attached to the rigid cage-like POSS on **P1-COOH**, complex **P1** containing **NBF14** tightly connected to a cubic POSS produced a larger leaning angle than that of **S1** (see Table 2). In addition, the strengthening of hydrogen bonding led to a close connection between **NBF14** and **P1-COOH**, which gave rise to an increasing leaning angle upon cooling (see Figure 6b).

Figures 7a and 7b are AFM phase images recorded from the thin-film samples of **P1** and **S1**, which were aligned with a DC electric field 0.8 V/μm in an in-plane-switching cell at 117 °C and followed by rapid quenching with liquid nitrogen to freeze the inner ribbon structures of the LC phase. Featuring the

DOI: 10.1021/acs.chemmater.5b00033
Chem. Mater. 2015, 27, 4525–4537

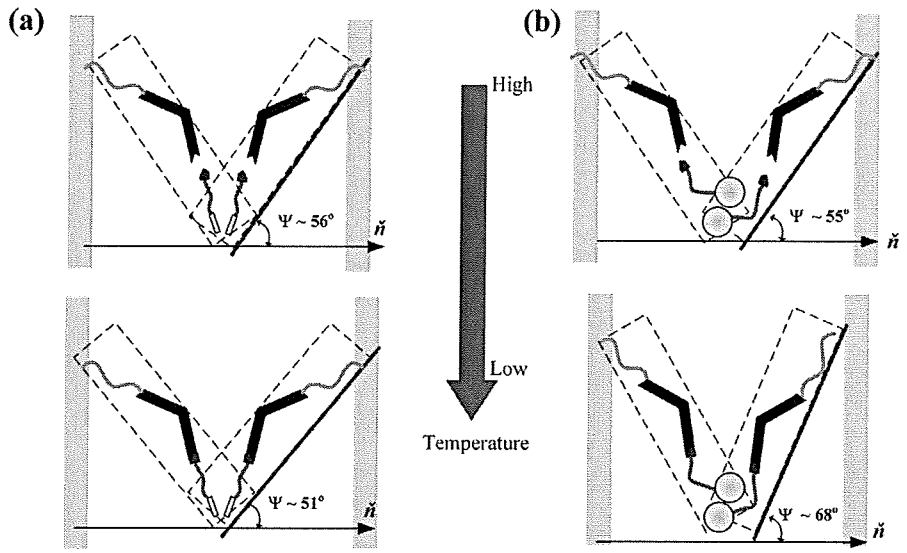

Figure 6. Schematic representations of molecular orientations (leaning angles) varying with temperature for (a) **S1** and (b) **P1**. Ψ: leaning angle and ň: layer normal.

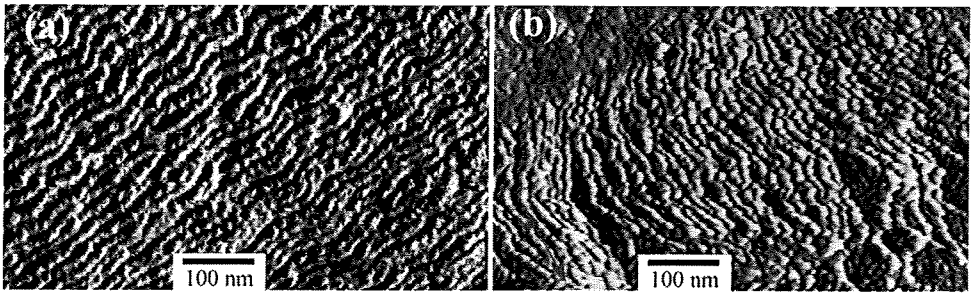

Figure 7. AFM phase images of (a) **P1** and (b) **S1**; red arrows indicate the alignment direction via the electric field.

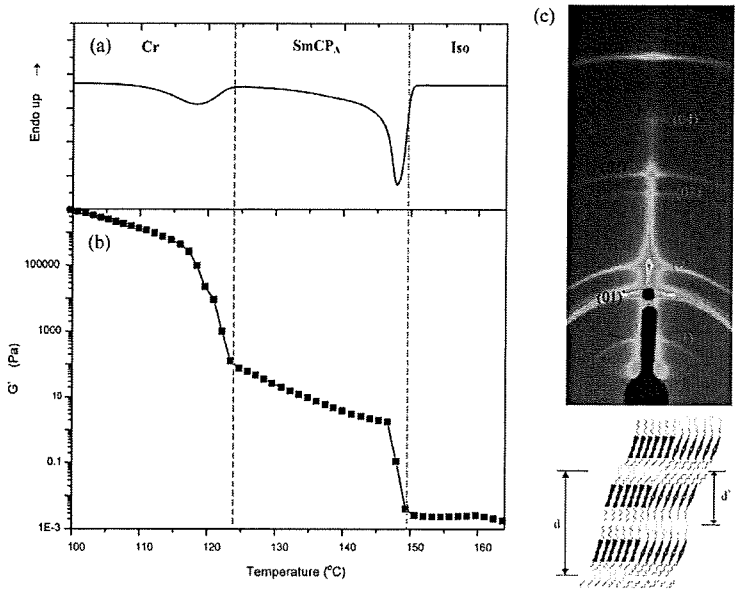

Figure 8. (a), (b) DSC trace and G' versus temperature upon cooling; (c) 2D GISAXS pattern of **C4** at 130 °C.

DOI: 10.1021/acs.chemmater.5b00033
Chem. Mater. 2015, 27, 4525−4537

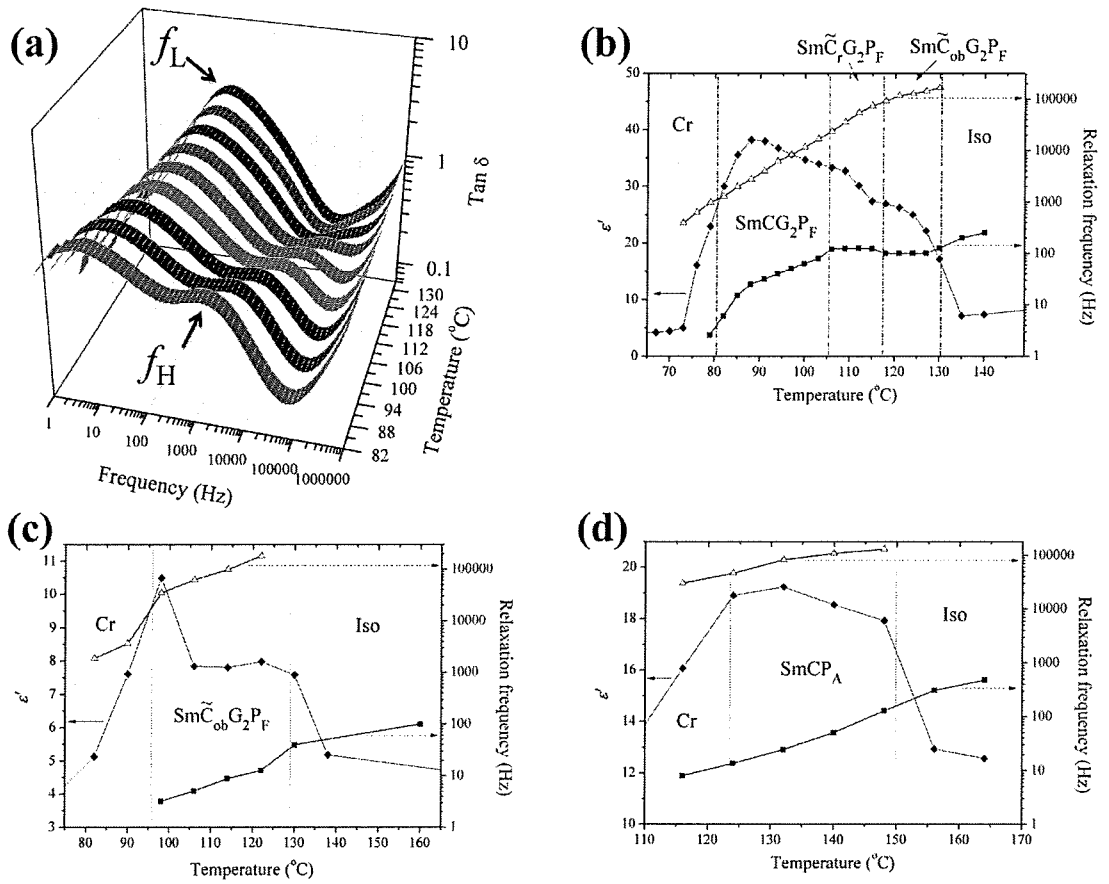

Figure 9. (a) Tan δ curves of **S1**; (b-d) f_H (open blue triangle), f_L (closed blue square), and the real part of the relative permittivity (closed black diamond) for **S1**, **P1**, and **C4**, respectively. The black solid and blue dashed arrows refer to ε' and relaxation curves, respectively.

$SmC_{ob}G_2P_F$ and $SmC_rG_2P_F$ phases for **P1** and **S1**, respectively, the bright domains in both AFM images exhibited regular periodicity of modulated ribbons aligned along the electric-field direction, marked as red arrows in Figures 7a and 7b. The average center-to-center distance (ca. 12 nm) between ribbons obtained from **S1** in Figure 7b is smaller than the average distance (ca. 17 nm) of **P1** in Figure 7a. These distances of AFM images correspond to the lattice parameters c (i.e., 12.10 and 16.29 nm, respectively) of **S1** and **P1** determined from GISAXS, indicating that the bright ribbon domains are composed of bilayer packing of the bent-core complexes (**S1** or **P1**). In the AFM image the dark domains also confirmed that defect zones existed between ribbons, which are in agreement with the expectation of electron density maps in Figures 4b and S3a'. The highly ordered ribbon structures on a large (i.e., submillimeter) scale indicated that the siloxane units could be fabricated into long thread-like aggregates by the self-assembly of the designed bent-core complexes.

From the above results, we have shown that the flexibility and geometric shape of siloxane pendants in **S1** and **P1** have a great influence on the molecular conformation of the bilayer packing in the SmCG-type structures. We further probed the mesophasic behavior in H-bonded complexes with multiple bent-core units confined by siloxane termini, such as **C4** and **P8**. Figure 8 demonstrates the DSC trace, dynamic shear modulus G', and GISAXS/GIWAXS patterns of complex **C4**. According to the DSC trace illustrated in Figure 8a, the exothermic onsets corresponded to the phase transition temperatures of Iso-LC and LC-Cr, which were also matched with the discontinuous points of the two-step-like curve in the dynamic shear modulus G' shown in Figure 8b. This result indicated that the mesophasic behavior of these complexes could be possibly verified by the characterization techniques of DSC and rheology meter. The detailed morphological properties could be further investigated by XRD measurements.

According to the GISAXS pattern of Figure 8c, two sets of lamellar reflections indexed by the Debye–Scherrer rings yield two layer d-spacing values, i.e., d = 9.23 and d' = 5.56 nm, which are smaller than the calculated molecular length of **C4** (ca. 12.5 nm), indicating a tilted molecular arrangement of the smectic C phase with a mixing of monolayer and bilayer packings for **C4**. Notably, just below the isotropic temperature (T_i) around 5 °C, only one lamellar reflection related to d' was found (see Figure S10), and both orders of d' and d occurred upon further cooling. It seems that only a part of H-bonded bent-core units attached to a ring-like siloxane terminus at high temperature, and, upon further cooling, four H-bonded bent-core units intended to connect to the ring-like siloxane terminus due to the strengthened H-bonding. Hence, the steric hindrance was enlarged to reduce the stacking of siloxane groups as well as to produce two orders of d' and d at low temperature, which also induced the complicated crystalline phase of **C4** compared to those of **S1** and **P1** (see Figure S2). Furthermore, the staggered packing of **C4** led to the difficulty

DOI: 10.1021/acs.chemmater.5b00033
Chem. Mater. 2015, 27, 4525–4537

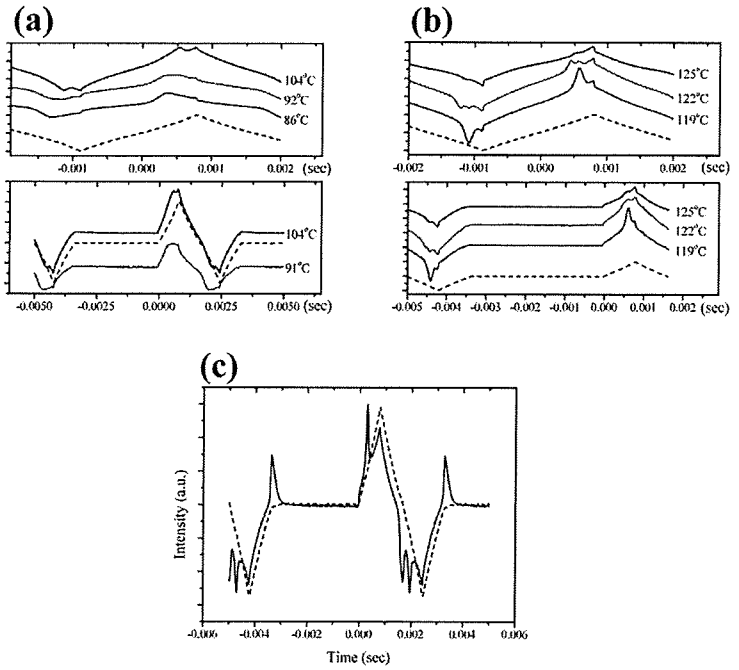

Figure 10. (a) **S1** and (b) **P1** under a triangular waveform (top charts) and a modified triangular waveform (bottom charts, after baseline normalizations) as well as (c) **C4** under a modified triangular waveform at 132 °C. The dashed lines indicate applied field 44.4 Vpp/μm, 300 Hz.

of obtaining tilt and leaning angles from the isotropic diffuse halo in the GIWAXS pattern (see the Supporting Information, Figure S11). For the same reason, among all H-bonded bent-core complexes **P8** is the only complex without any LC phase due to the largest steric hindrance and the confinement of eight bent-core units bound to the POSS unit. As a simple comparison, the shape effect of string-like and cage-like siloxane termini for **S1** and **P1** (with only one arm of H-bonded bent-core), respectively, caused their different types of SmCG phases. In addition, the confinement effect of **P1**, **C4**, and **P8** accompanied by increasing the numbers (from 1 to 4 and 8) of attached H-bonded bent-core arms resulted in the higher transition temperature and even the vanishing of mesophase for **P8**. In summary, the mesophasic behaviors were strongly affected by both shape and confinement effects.

Dielectric Relaxation of Mesophases. In three complexes **S1**, **P1**, and **C4** with mesophases, the tangent loss (Tan δ) curves exhibited two maxima within each mesophasic temperature range, where one of the representative dielectric Tan δ curves of **S1** upon cooling is illustrated in Figure 9a and the other cases as well as the relative permittivity (also named as complex dielectric constant) are shown in Figures S12 and S13 of the Supporting Information. Two relaxation frequencies of the Tan δ maxima at high frequency (f_H) and low frequency (f_L) as well as the real part of the relative permittivity (ε', at 500 Hz) versus temperature are summarized in Figures 9b-9d for **S1**, **P1**, and **C4**, respectively. The changes of ε' were consistent with phase transitions determined by G' curves (see Figures S3, 4, and 8). That is, the molecular conformation changes were able to affect not only mechanical but also dielectric performances[59−61] – even the subtle variation (such as subtypes of SmCG phases in **S1**) which was not detected by DSC and POM. Considering the temperature-dependent relations of f_L and f_H, we referred the slow relaxation of f_L to a molecular assembly of the phase transition and attributed the rapid relaxation of f_H to the responses of molecular rotation around the long axis.[55] Comparably, the f_L curve of **S1** in Figure 9b strongly reflects the ferroelectric SmCG-type phase sequence, i.e., $SmC\tilde{C}_{ob}G_2P_F$—$SmC\tilde{C}_rG_2P_F$—$SmCG_2P_F$, but the f_L curves of **P1** and **C4** in Figures 9c and 9d monotonically drop with decreasing temperature, featuring a single LC phase upon cooling. Monotonically decreasing f_H curve upon cooling is matched with no antiferroelectric-ferroelectric switching in the three complexes (to be shown next).[62]

Electro-Optical Behavior. The structural effects on the phase behavior, dielectric, and rheological properties of these H-bonded bent-core complexes have been analyzed, but the electro-optical properties of bent-core LCs, including spontaneous polarization (P_s) values as one of the important characteristics, need to be investigated for future applications. For instance, according to previous research[63−66] ferroelectrical liquid crystals (FLCs) with small viscosities and large P_s values are enabled for rapid responses: $\tau = \eta/(P_s \times E)$, in which τ is the response time, η is the rotational viscosity coefficient, and E is the applied electric field. The measurements of P_s values were based on the triangular-wave method[53] with frequency 300 Hz upon cooling. By applying a triangular wave upon cooling, a spontaneous polarization signal could be induced at the highest transition temperature (from isotropic to mesophase) of **S1** and **P1**. With further decreasing temperature, a second polarization signal near zero-field position of the triangular waveform appeared. As shown in the top charts of Figures 10a and 10b, the former signal was then weakened, while the second peak was reinforced. Unlike the H-bonded bent-core complex bearing a lateral attached siloxane terminal unit **H-SiO** reported previously,[51] though **S1** and **P1** with two signals revealed at approximately 92 and 122 °C, respectively, we still need to apply a modified triangular waveform (with a certain duration

DOI: 10.1021/acs.chemmater.5b00033
Chem. Mater. 2015, 27, 4525−4537

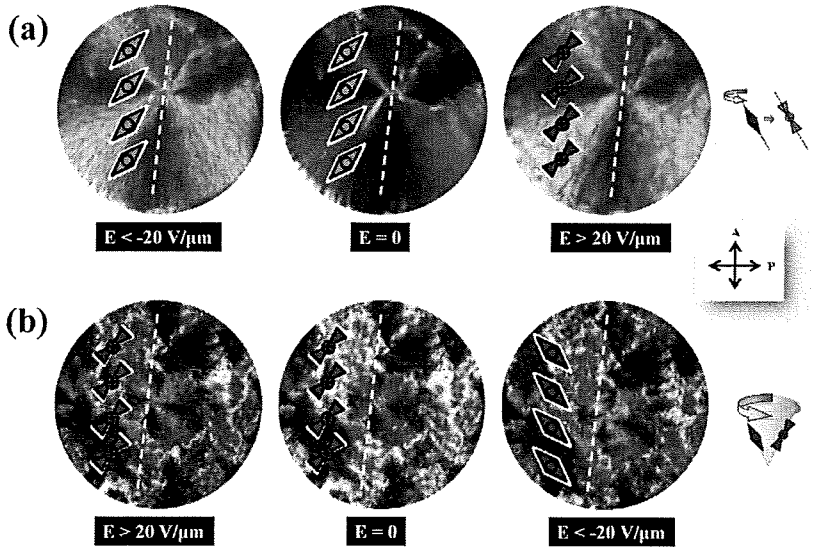

Figure 11. POM images (200×) of **S1** under crossed polarizers at (a) 120 °C and (b) 84 °C with zero and ±20 V/μm. The molecular rotations based on DC electric fields are illustrated.

of delay at zero voltage, see the bottom charts of Figures 10a and 10b) to confirm the ferroelectric or antiferroelectric switching behavior. Thus, according to the modified triangular waveform, we recognized them as a ferroelectric switching rather than an antiferroelectric behavior, which was verified by two split signals existing on the same side of the modified triangular waveform. On the contrary, **C4** showed not only two split signals at the zero voltage position but also at the edge of the waveform, indicating a typical antiferroelectric (AF) phase transition (see Figure 10c). Notably, the current peaks in Figures 10a and 10b were relatively broad and near the apex of triangular waveform. Usually, for ferroelectric switching siloxane based bent-core mesogens displaying rather sharp peaks were observed (like the current peaks in Figure 10c).[54,55,67−69] Hence, the switching behaviors of **S1** and **P1** were verified near the isotropicization temperature upon cooling as shown in Figure S14 of the Supporting Information. The responded current peaks were unobservable just above the isotopization temperatures for both **S1** and **P1** and appeared just below mesophasic temperature (also mesophases appeared from POM observation synchronous) indicated the formation of LC phases (instead of ionic impurities) leaded to the polar switching signals for **S1** and **P1**. Furthermore, the broad, apex-neared current peaks shown in Figures 10a and 10b were supposed to be related to the mesophases of **S1** and **P1**: in the columnar phases the polar switching might be suppressed by the ribbon structure and lead to delayed and broad polar signals.[51,67,70−75]

Compared with our previously published results of **H-SiO** with a lateral-attached string-like siloxane terminus, **S1** with an end-attached string-like siloxane terminus displayed a molecular switching behavior from rotating about its long axis (see Figure 11a) to the cone-shaped rotation (see Figure 11b), which differed from **H-SiO** under a DC electric field upon cooling.[51] On applying a DC electrical field of ±20 V/μm to **S1** at 120 °C, the extinction cross of the circular domain in the POM images of Figure 11a are unchanged (i.e., rotating about its long axis), but the extinction cross rotated 2−3° in Figure 11b under the DC field with another direction at 84 °C (i.e., doing a core-shaped rotation). As shown in Figure 11a, **S1** possessed a change of chirality represented as the color changes of the illustrated molecules at 120 °C from −20 V/μm to 20 V/μm. However, the chirality is independent of DC fields at 84 °C, in which the color of bent cores was the same under a reversed field (Figure 11b).[76−78] It means that the chirality of **S1** is possible to be tuned via temperature and DC fields for future applications. Visible circular domains with an extinction cross are not parallel to the polarizer and analyzer, indicating a synclinic arrangement. Both rotation mechanisms (along a cone or long axis in Figures 11a and 11b) were observed in some bent-core LCs, but the sequence dependence on temperature was not clear[76−78] -- even in compounds with similar structures (i.e., **S1** and **H-SiO**,[51] with end-attached and lateral-attached string-like siloxane termini, respectively).

Manipulation of B8 Phases by Binary Mixtures. Due to the different competition between both H-bonded interactions and nanosegregation of siloxane units, **S1** possessed a series of SmCG phase sequence. However, owing to a stronger shape effect of the cage-like siloxane units in **P1**, the 2D modulation of **P1** by the nanosegregation of POSS was stabilized to overcome the H-bonded interactions and thus to diminish the SmCG phase sequence. For future practical applications of the SmCG (B8) phase, it is of interest to modify and manipulate more mesomorphic properties in the binary blends composed of **S1** and **P1**. According to their colligative properties, the mesophasic ranges were obviously extended in the mixtures, which were determined by the experiments of GISAXS and rheology. With a higher concentration of **S1**, the binary mixture of **S1/P1_9/1** with 10 mol % **P1** dopant inherited the SmCG phase sequence, i.e., $Sm\tilde{C}_{ob}G_2P_F$—$Sm\tilde{C}_rG_2P_F$—$SmCG_2P_F$, as shown in Figures 12a and 12b, which exhibited a wider mesophasic range than **S1** homologue. Increasing the concentration of **P1**, both binary mixtures of **S1/P1_5/5** and **S1/P1_1/9** possessed sharp spot-like diffractions (Figures 12c and 12d) revealing that a relief of packing orders by the addition of **S1** led to the enhancement of 2D periodicities in the $Sm\tilde{C}_{ob}G_2P_F$ phase. In summary, the phase diagram of the discussed binary mixtures of **S1/P1** is depicted in Figure 12e,

DOI: 10.1021/acs.chemmater.5b00033
Chem. Mater. 2015, 27, 4525−4537

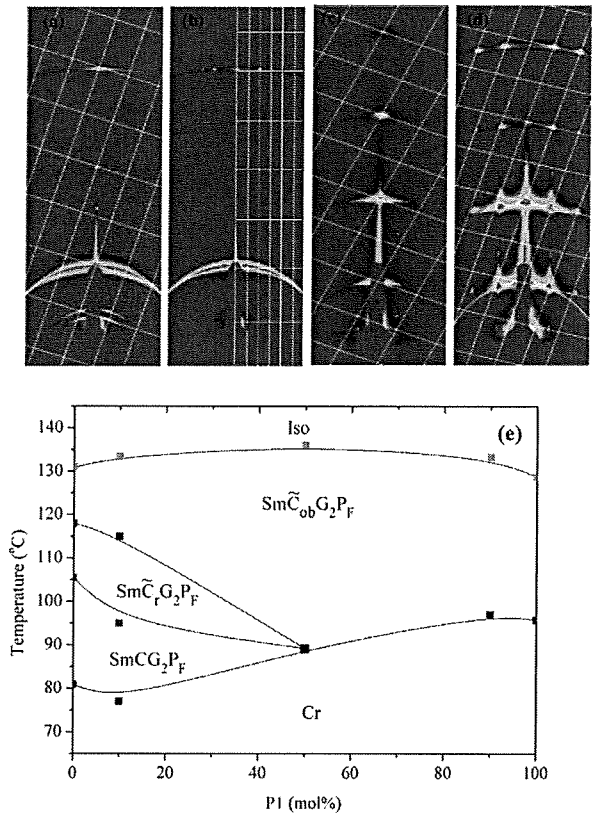

Figure 12. 2D GISAXS patterns for S1/P1_9/1 at (a) 125 °C and (b) 105 °C, S1/P1_5/5 at (c) 110 °C and S1/P1_1/9 at (d) 110 °C; (e) phase diagram of binary mixtures S1/P1 determined by GISAXS and rheology.

and the B8 phases were able to be controlled via the blending system through different (a) LC packing and (b) competition between both H-bonded interactions and nanosegregation of siloxane units.

To investigate and optimize the mesophasic and electro-optical properties of the binary mixtures, as shown in Figure S15 of the Supporting Information, the temperature dependent P_s and E_{th} (threshold electrical field) values were obtained from the spontaneous polarization measurements. According to Figure S15, the maximum P_s values (Max-P_s) and minimum E_{th} values (Min-Eth) within mesophasic ranges of all H-bonded bent-core complexes with polar orders (S1, P1, and C4) and their binary mixtures S1/P1 (with various molar ratios) are listed in Table 3. The mixtures showed greater Max-Ps values than those of monologues S1 and P1, presumably due to the long-range order of molecular assembly proven in Figures 12a-12d. The largest Max-Ps value, 512 nC/cm^2, in S1/P1_9/1 is attributed to an enhanced separation of dipoles by the dopant of P1 under the induced electric fields.[79] The least Min-Eth value, 10 Vpp/μm, in S1/P1_9/1 can result from the minor POSS doping so as to decrease the packing order of LC.[80] On the contrary, the largest E_{th} possessed in S1/P1_1/9 is attributed to alleviated packing order with a small addition of S1.[80] In general, the binary mixture of S1/P1_5/5 revealed a much larger Max-Ps, smaller Min-Eth, and broader mesophasic range than P1. In Figure 12c the single-crystal-like reflections of S1/P1_5/5 indicate a well aligned modulated ribbon phase ($SmC_{ob}G_2P_F$), which is, to our knowledge, a rare behavior of self-assembly in the bent-core LCs.

CONCLUSIONS

The H-bonded bent-core complexes attached to various terminal siloxane groups with string-, ring-, and cage-like shapes (i.e., linear siloxane unit −Si−O−Si−O−Si−, cyclic siloxane unit $(Si-O)_4$, and silsesquioxane unit POSS, respectively) were synthesized and studied. The shape effect of string-like and cage-like siloxane termini for S1 and P1 (with only one arm of H-bonded bent-core), respectively, caused their different types of SmCG phases and leaning angles. Moreover, their phase behaviors were investigated from the aspect of interplay between the H-bonding and nano-segregation of siloxane units in S1 and P1. In addition, by increasing the numbers of attached H-bonded bent-core arms in P1, C4, and P8, which were dominated by the confinement effect of several bent-core arms, resulted in higher transition temperatures and diminished mesophasic ranges. In analysis of polar orders, S1 and P1 showed ferroelectric transitions, but C4 displayed antiferroelectricity within the mesophasic range. AFM images of S1 and P1 demonstrate that a well ordered thread-like structure could be aligned by a DC field in the bilayer smectic CG phases, which indicated a potential application for nanoarrangements in the end-attached H-bonded bent-core complexes. Furthermore, the electro-optical performance of binary mixtures of S1 and P1 (with various molar ratios) could be optimized via doping a minor ratio of P1 into S1 (i.e., S1/P1_9/1). Finally, S1/P1_5/5 with single-crystal-like reflections pointed out a well aligned modulated ribbon phase. Accordingly, these findings provide a new strategy to obtain specific mesophases (including the B8 phases) possessing high P_s and low E_{th} values as well as nanoarrangements by the self-assembly of bent-core complexes bearing specifically designed terminal groups.

ASSOCIATED CONTENT

Supporting Information

The details of synthetic steps and the elemental characterization of S1-COOH, P1-COOH, C4-COOH, P8-COOH, and NBF14; the setup for P_s value measurement; the mesophasic determination of S1; GISAXS patterns of S1, P1, and C4 in crystalline phase; the tilt and leaning angle sets of S1

Table 3. Electro-Optical Properties and Mesophasic Ranges of All H-Bonded Bent-Core Complexes with Polar Orders (S1, P1, and C4) and Their Binary Mixtures S1/P1 (with Various Molar Ratios)

compd	S1	S1/P1_9/1[a]	S1/P1_5/5[a]	S1/P1_1/9[a]	P1	C4
Max-Ps (nC/cm^2)	347.6	512.2	304.0	244.0	156.0	322.9
Min-Eth (Vpp/μm)	15.0	10.4	20.4	33.3	21.2	11.3
mesophase range (°C)	58.3	60.7	46.8	36.3	33.0	26.8

[a]S1/P1_x/y: the symbol x/y means the molar ratio of S1/P1.

DOI: 10.1021/acs.chemmater.5b00033
Chem. Mater. 2015, 27, 4525−4537

and **P1**; phase transition temperatures and enthalpies of **S1**, **P1**, **C4**, and **P8** with information on the polar order; other Tan δ curves, SAXS patterns, and P_s value measurement of **S1**, **P1**, and **C4** mentioned in the text. The Supporting Information is available free of charge on the ACS Publications website at DOI: 10.1021/acs.chemmater.5b00033.

AUTHOR INFORMATION

Corresponding Authors

*E-mail: weitsung@nsrrc.org.tw.
*E-mail: linhc@mail.nctu.edu.tw.

Notes

The authors declare no competing financial interest.

ACKNOWLEDGMENTS

Financial support of this project was provided by the Ministry of Science and Technology (MOST) through MOST 103-2113-M-009-018-MY3 and MOST 103-2221-E-009-215-MY3. We thank Drs. Hwo-Shuenn Sheu, U-Ser Jeng, Jey-Jau Lee, and Yao-Chang Lee for assistance with the XRD measurements at BL01C2, 23A1, 17A1, and 14A1 at the National Synchrotron Radiation Research Center (NSRRC) in Taiwan.

REFERENCES

(1) Pelzl, G.; Wirth, I.; Weissflog, W. The First 'banana Phase' found in an Original Vorländer Substance. *Liq. Cryst.* **2001**, *28*, 969–972.

(2) Vorländer, D.; Apel, A. Die Richtung Der Kohlenstoff-Valenzen in Benzolabkömmlingen (Ii.). *Ber. Dtsch. Chem. Ges.* **1932**, *65*, 1101–1109.

(3) Niori, T.; Sekine, T.; Watanabe, J.; Furukawa, T.; Takezoe, H. Distinct Ferroelectric Smectic Liquid Crystals Consisting of Banana Shaped Achiral Molecules. *J. Mater. Chem.* **1996**, *6*, 1231–1233.

(4) Sekine, T.; Niori, T.; Watanabe, J.; Furukawa, T.; Choi, S. W.; Takezoe, H. Spontaneous Helix Formation in Smectic Liquid Crystals Comprising Achiral Molecules. *J. Mater. Chem.* **1997**, *7*, 1307–1309.

(5) Thisayukta, J.; Niwano, H.; Takezoe, H.; Watanabe, J. Enhancement of Twisting Power in the Chiral Nematic Phase by Introducing Achiral Banana-Shaped Molecules. *J. Am. Chem. Soc.* **2002**, *124*, 3354–3358.

(6) Takezoe, H.; Takanishi, Y. Bent-Core Liquid Crystals: Their Mysterious and Attractive World. *Jpn. J. Appl. Phys.* **2006**, *45*, 597–625.

(7) Reddy, R. A.; Tschierske, C. Bent-Core Liquid Crystals: Polar Order, Superstructural Chirality and Spontaneous Desymmetrisation in Soft Matter Systems. *J. Mater. Chem.* **2006**, *16*, 907–961.

(8) Shimbo, Y.; Takanishi, Y.; Ishikawa, K.; Gorecka, E.; Pociecha, D.; Mieckowski, J.; Gomola, K.; Takezoe, H. Ideal Liquid Crystal Display Mode Using Achiral Banana-Shaped Liquid Crystals. *Jpn. J. Appl. Phys.* **2006**, *45*, L282–L284.

(9) Nair, G. G.; Bailey, C. A.; Taushanoff, S.; Fodor-Csorba, K.; Vajda, A.; Varga, Z.; Bota, A.; Jakli, A. Electrically Tunable Color by Using Mixtures of Bent-Core and Rod-Shaped Molecules. *Adv. Mater.* **2008**, *20*, 3138–3142.

(10) Jákli, A. Scattering Displays from 'Banana-Smectics'. *Liquid Crystals Today* **2002**, *11*, 1–5.

(11) Jákli, A.; Chien, L. C.; Kruerke, D.; Rauch, S.; Sawadw, H.; Bault, P.; Heppke, G.; Fodor-Csorba, K.; Nair, G. G. Light Shutters and Electro-Optical Storage Devices from Antiferroelectric Liquid Crystals of Bent-Shape Molecules. In *Liquid Crystal Materials, Devices, and Applications Ix*; Chien, L. C., Ed.; 2003; Vol. *5003*, pp 73–80.

(12) Pintre, I. C.; Luis Serrano, J.; Blanca Ros, M.; Martinez-Perdiguero, J.; Alonso, I.; Ortega, J.; Folcia, C. L.; Etxebarria, J.; Alicante, R.; Villacampa, B. Bent-Core Liquid Crystals in a Route to Efficient Organic Nonlinear Optical Materials. *J. Mater. Chem.* **2010**, *20*, 2965–2971.

(13) Iglesias, W.; Abbott, N. L.; Mann, E. K.; Jákli, A. Improving Liquid-Crystal-Based Biosensing in Aqueous Phases. *ACS Appl. Mater. Interfaces* **2012**, *4*, 6883–6889.

(14) Jákli, A.; Pintre, I. C.; Luis Serrano, J.; Blanco Ros, M.; Rosario de la Fuente, M. Piezoelectric and Electric-Field-Induced Properties of a Ferroelectric Bent-Core Liquid Crystal. *Adv. Mater.* **2009**, *21*, 3784–3788.

(15) Callahan, R. A.; Coffey, D. C.; Chen, D.; Clark, N. A.; Rumbles, G.; Walba, D. M. Charge Generation Measured for Fullerene-Helical Nanofilament Liquid Crystal Heterojunctions. *ACS Appl. Mater. Interfaces* **2014**, *6*, 4823–4830.

(16) Chiang, I. H.; Long, C.-J.; Lin, H.-C.; Chuang, W.-T.; Lee, J.-J.; Lin, H.-C. Broad Ranges and Fast Responses of Single-Component Blue-Phase Liquid Crystals Containing Banana-Shaped 1,3,4-Oxadiazole Cores. *ACS Appl. Mater. Interfaces* **2014**, *6*, 228–235.

(17) Park, K.-W.; Gim, M.-J.; Kim, S.; Hur, S.-T.; Choi, S.-W. Liquid-Crystalline Blue Phase Ii System Comprising a Bent-Core Molecule with a Wide Stable Temperature Range. *ACS Appl. Mater. Interfaces* **2013**, *5*, 8025–8029.

(18) Gonzalez, L.; Gimeno, N.; Maria Tejedor, R.; Polo, V.; Blanca Ros, M.; Uriel, S.; Luis Serrano, J. Halogen-Bonding Complexes Based on Bis(Iodoethynyl)Benzene Units: A New Versatile Route to Supramolecular Materials. *Chem. Mater.* **2013**, *25*, 4503–4510.

(19) Gimeno, N.; Vergara, J.; Cano, M.; Luis Serrano, J.; Blanca Ros, M.; Ortega, J.; Folcia, C. L.; Rodriguez-Conde, S.; Sanz-Enguita, G.; Etxebarria, J. Janus-Type Dendromesogens: A Tool to Control the Nanosegregation and Polar Organization of Bent-Core Structures. *Chem. Mater.* **2013**, *25*, 286–296.

(20) Vergara, J.; Gimeno, N.; Cano, M.; Barbera, J.; Romero, P.; Luis Serrano, J.; Ros, M. B. Mesomorphism from Bent-Core Based Ionic Dendritic Macromolecules. *Chem. Mater.* **2011**, *23*, 4931–4940.

(21) Seltmann, J.; Marini, A.; Mennucci, B.; Dey, S.; Kumar, S.; Lehmann, M. Nonsymmetric Bent-Core Liquid Crystals Based on a 1,3,4-Thiadiazole Core Unit and Their Nematic Mesomorphism. *Chem. Mater.* **2011**, *23*, 2630–2636.

(22) Vita, F.; Tauscher, T.; Speetjens, F.; Samulski, E. T.; Scharrer, E.; Francescangeli, O. Evidence of Biaxial Order in the Cybotactic Nematic Phase of Bent-Core Mesogens. *Chem. Mater.* **2014**, *26*, 4671–4674.

(23) Singh, H.; Balamurugan, A.; Jayakannan, M. Solid State Assemblies and Photophysical Characteristics of Linear and Bent-Core Pi-Conjugated Oligophenylenevinylenes. *ACS Appl. Mater. Interfaces* **2013**, *5*, 5578–5591.

(24) Pelzl, G.; Diele, S.; Weissflog, W. Banana-Shaped Compounds - a New Field of Liquid Crystals. *Adv. Mater.* **1999**, *11*, 707–724.

(25) Lee, S. K.; Heo, S.; Lee, J. G.; Kang, K. T.; Kumazawa, K.; Nishida, K.; Shimbo, Y.; Takanishi, Y.; Watanabe, J.; Doi, T.; Takahashi, T.; Takezoe, H. Odd-Even Behavior of Ferroelectricity and Antiferroelectricity in Two Homologous Series of Bent-Core Mesogens. *J. Am. Chem. Soc.* **2005**, *127*, 11085–11091.

(26) Otani, T.; Araoka, F.; Ishikawa, K.; Takezoe, H. Enhanced Optical Activity by Achiral Rod-Like Molecules Nanosegregated in the B-4 Structure of Achiral Bent-Core Molecules. *J. Am. Chem. Soc.* **2009**, *131*, 12368–12372.

(27) Chen, D.; Maclennan, J. E.; Shao, R.; Yoon, D. K.; Wang, H.; Korblova, E.; Walba, D. M.; Glaser, M. A.; Clark, N. A. Chirality-Preserving Growth of Helical Filaments in the B4 Phase of Bent-Core Liquid Crystals. *J. Am. Chem. Soc.* **2011**, *133*, 12656–12663.

(28) Coleman, D. A.; Fernsler, J.; Chattham, N.; Nakata, M.; Takanishi, Y.; Korblova, E.; Link, D. R.; Shao, R. F.; Jang, W. G.; Maclennan, J. E.; Mondainn-Monval, O.; Boyer, C.; Weissflog, W.; Pelzl, G.; Chien, L. C.; Zasadzinski, J.; Watanabe, J.; Walba, D. M.; Takezoe, H.; Clark, N. A. Polarization-Modulated Smectic Liquid Crystal Phases. *Science* **2003**, *301*, 1204–1211.

(29) Pelz, K.; Weissflog, W.; Baumeister, U.; Diele, S. Various Columnar Phases Formed by Bent-Core Mesogens. *Liq. Cryst.* **2003**, *30*, 1151–1158.

(30) Walba, D. M.; Korblova, E.; Shao, R.; Maclennan, J. E.; Link, D. R.; Glaser, M. A.; Clark, N. A. A Ferroelectric Liquid Crystal

DOI: 10.1021/acs.chemmater.5b00033
Chem. Mater. 2015, 27, 4525–4537

Conglomerate Composed of Racemic Molecules. *Science* **2000**, *288*, 2181−2184.
(31) Sekine, T.; Niori, T.; Sone, M.; Watanabe, J.; Choi, S. W.; Takanishi, Y.; Takezoe, H. Origin of Helix in Achiral Banana-Shaped Molecular Systems. *Jpn. J. Appl. Phys.* **1997**, *36*, 6455−6463.
(32) Thisayukta, J.; Takezoe, H.; Watanabe, J. Study on Helical Structure of the B-4 Phase Formed from Achiral Banana-Shaped Molecule. *Jpn. J. Appl. Phys.* **2001**, *40*, 3277−3287.
(33) Takanishi, Y.; Ishikawa, K.; Watanabe, J.; Takezoe, H.; Yamashita, M.; Kawase, K. Terahertz Spectroscopy in Smectic Phases of a Bent-Core Molecule. *Phys. Rev. E* **2005**, *71*, 061701.
(34) Zep, A.; Sitkowska, K.; Pociecha, D.; Gorecka, E. Photoresponsive Helical Nanofilaments of B-4 Phase. *J. Mater. Chem. C* **2014**, *2*, 2323−2327.
(35) Zhang, C.; Diorio, N.; Lavrentovich, O. D.; Jakli, A. Helical Nanofilaments of Bent-Core Liquid Crystals with a Second Twist. *Nat. Commun.* **2014**, *5*, 3302.
(36) Diele, S.; Grande, S.; Kruth, H.; Lischka, C. H.; Pelzi, G.; Weissflog, W.; Wirth, I. Structure and Properties of Liquid Crystalline Phases Formed by Achiral Banana-Shaped Molecules. *Ferroelectrics* **1998**, *212*, 169−177.
(37) Shen, D.; Diele, S.; Pelzl, G.; Wirth, I.; Tschierske, C. Designing Banana-Shaped Liquid Crystals without Schiff's Base Units: M-Terphenyls, 2,6-Diphenylpyridines and V-Shaped Tolane Derivatives. *J. Mater. Chem.* **1999**, *9*, 661−672.
(38) Weissflog, W.; Wirth, I.; Diele, S.; Pelzl, G.; Schmalfuss, H.; Schoss, T.; Wurflinger, A. The N,N′-Bis 4-(4-N-Alkyloxybenzoyloxy)-Benzylidene Phenylene-1,3-Diamines: Mesophase Behaviour and Physical Properties. *Liq. Cryst.* **2001**, *28*, 1603−1609.
(39) Weissflog, W.; Lischka, C.; Benne, L.; Scharf, T.; Pelzl, G.; Diele, S.; Kruth, H. New Banana-Shaped Mesogens. In *Liquid Crystals: Chemistry and Structure*; Tykarska, M., Dabrowski, R., Zielinski, J., Eds.; 1998; Vol. 3319, pp 14−19.
(40) Pelzl, G.; Diele, S.; Jákli, A.; Lischka, C.; Wirth, I.; Weissflog, W. Helical Superstructures in a Novel Smectic Mesophase Formed by Achiral Banana-Shaped Molecules. *Liq. Cryst.* **1999**, *26*, 135−139.
(41) Jákli, A.; Lischka, C.; Weissflog, W.; Pelzl, G.; Saupe, A. Helical Filamentary Growth in Liquid Crystals Consisting of Banana-Shaped Molecules. *Liq. Cryst.* **2000**, *27*, 1405−1409.
(42) Chen, D.; Yoon, D. K.; Maclennan, J. E.; Glaser, M. A.; Korblova, E.; Walba, D. M.; Gimeno, N.; Blanca Ros, M.; Deb, R.; Rao, N. V. S.; Clark, N. A. Spiral Layer Undulation Defects in B7 Liquid Crystals. *Soft Matter* **2013**, *9*, 11303−11308.
(43) De Gennes, P.-G.; Prost, J. *The Physics of Liquid Crystals*; Clarendon Press Oxford: 1993.
(44) Bedel, J. P.; Rouillon, J. C.; Marcerou, J. P.; Nguyen, H. T.; Achard, M. F. Evidence for Different Polymorphisms with and without an External Electric Field in a Series of Bent-Shaped Molecules. *Phys. Rev. E* **2004**, *69*, 061702.
(45) Bedel, J. P.; Rouillon, J. C.; Marcerou, J. P.; Laguerre, M.; Nguyen, H. T.; Achard, M. F. New Switchable Smectic Phases in Banana-Shaped Compounds. *Liq. Cryst.* **2001**, *28*, 1285−1292.
(46) Nguyen, H. T.; Bedel, J. P.; Rouillon, J. C.; Marcerou, J. P.; Achard, M. F. Banana-Shaped Molecules Derived from Substituted Isophthalic Acids. *Pramana* **2003**, *61*, 395−404.
(47) Brand, H. R.; Cladis, P. E.; Pleiner, H. Macroscopic Properties of Smectic C-G Liquid Crystals (Vol 6, Pg 347, 1998). *Eur. Phys. J. B* **2003**, *31*, 147−147.
(48) Pociecha, D.; Vaupotic, N.; Gorecka, E.; Mieczkowski, J.; Gomola, K. 2-D Density-Modulated Structures in Asymmetric Bent-Core Liquid Crystals. *J. Mater. Chem.* **2008**, *18*, 881−885.
(49) Gorecka, E.; Pociecha, D.; Vaupotic, N.; Cepic, M.; Gomola, K.; Mieczkowski, J. Modulated General Tilt Structures in Bent-Core Liquid Crystals. *J. Mater. Chem.* **2008**, *18*, 3044−3049.
(50) Vaupotic, N.; Pociecha, D.; Cepic, M.; Gomola, K.; Mieczkowski, J.; Gorecka, E. Evidence for General Tilt Columnar Liquid Crystalline Phase. *Soft Matter* **2009**, *5*, 2281−2285.
(51) Chen, W.-H.; Chuang, W.-T.; Jeng, U. S.; Sheu, H.-S.; Lin, H.-C. New Smcg Phases in a Hydrogen-Bonded Bent-Core Liquid Crystal Featuring a Branched Siloxane Terminal Group. *J. Am. Chem. Soc.* **2011**, *133*, 15674−15685.
(52) Keith, C.; Dantlgraber, G.; Reddy, R. A.; Baumeister, U.; Prehm, M.; Hahn, H.; Lang, H.; Tschierske, C. The Influence of Shape and Size of Silyl Units on the Properties of Bent-Core Liquid Crystals - from Dimers Via Oligomers and Dendrimers to Polymers. *J. Mater. Chem.* **2007**, *17*, 3796−3805.
(53) Miyasato, K.; Abe, S.; Takezoe, H.; Fukuda, A.; Kuze, E. Direct Method with Triangular Waves for Measuring Spontaneous Polarization in Ferroelectric Liquid-Crystals. *Jpn. J. Appl. Phys.* **1983**, *22*, L661−L663.
(54) Geese, K.; Prehm, M.; Tschierske, C. Bent-Core Mesogens with Thiophene Units. *J. Mater. Chem.* **2010**, *20*, 9658−9665.
(55) Keith, C.; Reddy, R. A.; Prehm, M.; Baumeister, U.; Kresse, H.; Chao, J. L.; Hahn, H.; Lang, H.; Tschierske, C. Layer Frustration, Polar Order and Chirality in Liquid Crystalline Phases of Silyl-Terminated Achiral Bent-Core Molecules. *Chem.—Eur. J.* **2007**, *13*, 2556−2577.
(56) Keith, C.; Reddy, R. A.; Baumeister, U.; Tschierske, C. Banana-Shaped Liquid Crystals with Two Oligosiloxane End-Groups: Field-Induced Switching of Supramolecular Chirality. *J. Am. Chem. Soc.* **2004**, *126*, 14312−14313.
(57) Kato, T.; Frechet, J. M. J.; Wilson, P. G.; Saito, T.; Uryu, T.; Fujishima, A.; Jin, C.; Kaneuchi, F. Hydrogen-Bonded Liquid-Crystals - Novel Mesogens Incorporating Nonmesogenic Bipyridyl Compounds through Complexation between H-Bond Donor and Acceptor Moieties. *Chem. Mater.* **1993**, *5*, 1094−1100.
(58) Grill, A. Porous Psicoh Ultralow-K Dielectrics for Chip Interconnects Prepared by Pecvd. *Annu. Rev. Mater. Res.* **2009**, *39*, 49−69.
(59) Nakata, M.; Link, D. R.; Thisayukta, J.; Takanishi, Y.; Ishikawa, K.; Watanabe, J.; Takezoe, H. Frustration of Polarity and Chirality in a Binary Mixture of Bent-Core Mesogens. *J. Mater. Chem.* **2001**, *11*, 2694−2699.
(60) Bailey, C.; Fodor-Csorba, K.; Gleeson, J. T.; Sprunt, S. N.; Jakli, A. Rheological Properties of Bent-Core Liquid Crystals. *Soft Matter* **2009**, *5*, 3618−3622.
(61) Chakraborty, A.; Das, M. K.; Das, B.; Lehmann, A.; Tschierske, C. Rotational Viscosity Measurements of Bent-Core Nematogens. *Soft Matter* **2013**, *9*, 4273−4283.
(62) Chalapathi, P. V.; Srinivasulu, M.; Goud, B. V. S.; Pisipati, V.; Potukuchi, D. M. Synthesis, Characterization, Spontaneous Polarization and Dielectric Relaxation Studies in the Antiferroelectric and Ferroelectric Phases of an Achiral Banana Liquid Crystal: Bent-16. *Ferroelectrics* **2005**, *322*, 53−67.
(63) Kimura, S.; Nishiyama, S.; Ouchi, Y.; Takezoe, H.; Fukuda, A. Viscosity Measurement in Ferroelectric Liquid-Crystals Using a Polarization Switching Current. *Jpn. J. Appl. Phys.* **1987**, *26*, L255−L257.
(64) Okada, H.; Sakurai, T.; Katoh, T.; Watanabe, M.; Onnagawa, H.; Nakatani, N.; Miyashita, K. Electrooptic Responses of Antiferroelectric Liquid-Crystals with Very Short Reverse Pulse Voltage. *Jpn. J. Appl. Phys.* **1993**, *32*, 4339−4343.
(65) Okada, H.; Kurabayashi, K.; Kidoh, Y.; Onnagawa, H.; Miyashita, K. Video-Rate Operation in High-Speed Smectic Liquid-Crystal Light-Modulator. *Jpn. J. Appl. Phys.* **1994**, *33*, 4666−4672.
(66) Essid, S.; Manai, M.; Gharbi, A.; Marcerou, J. P.; Rouillon, J. C. Electro-Optical Switching Properties for Measuring the Parameters of a Ferroelectric Liquid Crystal. *Liq. Cryst.* **2005**, *32*, 307−313.
(67) Keith, C.; Reddy, R. A.; Hauser, A.; Baumeister, U.; Tschierske, C. Silicon-Containing Polyphilic Bent-Core Molecules: The Importance of Nanosegregation for the Development of Chirality and Polar Order in Liquid Crystalline Phases Formed by Achiral Molecules. *J. Am. Chem. Soc.* **2006**, *128*, 3051−3066.
(68) Keith, C.; Reddy, R. A.; Hahn, H.; Lang, H.; Tschierske, C. The Carbosilane Unit as a Stable Building Block for Liquid Crystal Design: A New Class of Ferroelectric Switching Banana-Shaped Mesogens. *Chem. Commun.* **2004**, 1898−1899.

DOI: 10.1021/acs.chemmater.5b00033
Chem. Mater. 2015, 27, 4525−4537

(69) Dantlgraber, G.; Eremin, A.; Diele, S.; Hauser, A.; Kresse, H.; Pelzl, G.; Tschierske, C. Chirality and Macroscopic Polar Order in a Ferroelectric Smectic Liquid-Crystalline Phase Formed by Achiral Polyphilic Bent-Core Molecules. *Angew. Chem., Int. Ed.* **2002**, *41*, 2408−2412.
(70) Kardas, D.; Prehm, M.; Baumeister, U.; Pociecha, D.; Reddy, R. A.; Mehl, G. H.; Tschierske, C. End Functionalised Liquid Crystalline Bent-Core Molecules and First Dab Derived Dendrimers with Banana Shaped Mesogenic Units. *J. Mater. Chem.* **2005**, *15*, 1722−1733.
(71) Szydlowska, J.; Mieczkowski, J.; Matraszek, J.; Bruce, D. W.; Gorecka, E.; Pociecha, D.; Guillon, D. Bent-Core Liquid Crystals Forming Two- and Three-Dimensional Modulated Structures. *Phys. Rev. E* **2003**, *67*, 031702.
(72) Bedel, J. P.; Rouillon, J. C.; Marcerou, J. P.; Laguerre, M.; Nguyen, H. T.; Achard, M. F. Influence of Fluoro Substituents on the Mesophase Behaviour of Banana-Shaped Molecules. *J. Mater. Chem.* **2002**, *12*, 2214−2220.
(73) Bedel, J. P.; Rouillon, J. C.; Marcerou, J. P.; Laguerre, M.; Nguyen, H. T.; Achard, M. F. Novel Mesophases in Fluorine Substituted Banana-Shaped Mesogens. *Liq. Cryst.* **2000**, *27*, 1411−1421.
(74) Umadevi, S.; Sadashiva, B. K.; Murthy, H. N. S.; Raghunathan, V. A. Mesogenic Dimers Composed of Bent-Core Molecules with Flexible Alkylene Spacer. *Soft Matter* **2006**, *2*, 210−214.
(75) Reddy, R. A.; Baumeister, U.; Keith, C.; Hahn, H.; Lang, H.; Tschierske, C. Influence of the Core Structure on the Development of Polar Order and Superstructural Chirality in Liquid Crystalline Phases Formed by Silylated Bent-Core Molecules: Lateral Substituents. *Soft Matter* **2007**, *3*, 558−570.
(76) Reddy, R. A.; Schroder, M. W.; Bodyagin, M.; Kresse, H.; Diele, S.; Pelzl, G.; Weissflog, W. Field-Induced Switching of Chirality in Undulated Ferroelectric and Antiferroelectric Smcp Phases Formed by Bent-Core Mesogens. *Angew. Chem., Int. Ed.* **2005**, *44*, 774−778.
(77) Weissflog, W.; Dunemann, U.; Schroder, M. W.; Diele, S.; Pelzl, G.; Kresse, H.; Grande, S. Field-Induced Inversion of Chirality in Smcpa Phases of New Achiral Bent-Core Mesogens. *J. Mater. Chem.* **2005**, *15*, 939−946.
(78) Zhang, Y.; Baumeister, U.; Tschierske, C.; O'Callaghan, M. J.; Walker, C. Achiral Bent-Core Molecules with a Series of Linear or Branched Carbosilane Termini: Dark Conglomerate Phases, Supramolecular Chirality and Macroscopic Polar Order. *Chem. Mater.* **2010**, *22*, 2869−2884.
(79) Singh, D. P.; Gupta, S. K.; Manohar, R. Znol-Xsx Nanosphere in Ferroelectric Liquid Crystal Matrix: The Effect of Aggregation and Defects on the Dielectric and Electro-Optical Properties. *Adv. Condens. Matter Phys.* **2013**, 250301.
(80) Zhang, T.; Zhong, C.; Xu, J. Cds-Nanoparticle-Doped Liquid Crystal Displays Showing Low Threshold Voltage. *Jpn. J. Appl. Phys.* **2009**, *48*, 055002.

DOI: 10.1021/acs.chemmater.5b00033
Chem. Mater. 2015, 27, 4525−4537